How to cite: *Angew. Chem. Int. Ed.* **2022,** *61,* e202116517
International Edition: doi.org/10.1002/anie.202116517
German Edition: doi.org/10.1002/ange.202116517

CO_2 Hydrogenation

Identifying Performance Descriptors in CO_2 Hydrogenation over Iron-Based Catalysts Promoted with Alkali Metals

*Qingxin Yang, Vita A. Kondratenko, Sergey A. Petrov, Dmitry E. Doronkin, Erisa Saraçi, Henrik Lund, Aleks Arinchtein, Ralph Kraehnert, Andrey S. Skrypnik, Alexander A. Matvienko, and Evgenii V. Kondratenko**

Abstract: Alkali metal promoters have been widely employed for preparation of heterogeneous catalysts used in many industrially important reactions. However, the fundamentals of their effects are usually difficult to access. Herein, we unravel mechanistic and kinetic aspects of the role of alkali metals in CO_2 hydrogenation over Fe-based catalysts through state-of-the-art characterization techniques, spatially resolved steady-state and transient kinetic analyses. The promoters affect electronic properties of iron in iron carbides. These carbide characteristics determine catalyst ability to activate H_2, CO and CO_2. The Allen scale electronegativity of alkali metal promoter was successfully correlated with the rates of CO_2 hydrogenation to higher hydrocarbons and CH_4 as well as with the rate constants of individual steps of CO or CO_2 activation. The derived knowledge can be valuable for designing and preparing catalysts applied in other reactions where such promoters are also used.

[*] Q. Yang, Dr. V. A. Kondratenko, Dr. H. Lund, A. S. Skrypnik, Prof. Dr. E. V. Kondratenko
Leibniz-Institut für Katalyse e. V.
Albert-Einstein-Str. 29a, 18059 Rostock (Germany)
E-mail: Evgenii.Kondratenko@catalysis.de

S. A. Petrov, A. S. Skrypnik, Dr. A. A. Matvienko
Institute of Solid-State Chemistry and Mechanochemistry
Kutateladze Str. 18, 630128 Novosibirsk (Russia)

Dr. D. E. Doronkin, Dr. E. Saraçi
Institute of Catalysis Research and Technology (IKFT), Karlsruhe Institute of Technology
Herrmann-von-Helmholtz-Platz 1, 76344 Eggenstein-Leopoldshafen (Germany)

A. Arinchtein, Dr. R. Kraehnert
Department of Chemistry, Technische Universität Berlin
Strasse des 17. Juni 124, 10623 Berlin (Germany)

A. S. Skrypnik, Dr. A. A. Matvienko
Novosibirsk State University
Pirogova Str. 1, 630090 Novosibirsk (Russia)

Introduction

Greenhouse gases released upon human activities are generally recognized to contribute to the global warming and climate changes. CO_2 emissions from burning fossil fuels are the main contributors to this situation. The utilization of this greenhouse gas as a feedstock in the chemical industry is a promising way to close the carbon cycle and provides a solution for the above-mentioned ecological problems.[1] One attractive approach is CO_2 conversion into chemicals or fuels with H_2 derived from H_2O using renewable electricity.[2] To produce hydrocarbons, CO_2 can be hydrogenated to methanol over one catalyst followed by the conversion of the latter into lower olefins over another catalyst.[3] Alternatively, one catalyst can convert CO_2 into CO via the reverse water gas shift (RWGS) reaction and subsequently hydrogenate CO to C_{2+}-hydrocarbons through the classical Fischer–Tropsch synthesis (CO-FTS).[4] This approach is known as CO_2 Fischer–Tropsch synthesis (CO_2-FTS).

As in CO-FTS related studies, Co- or Fe-based catalysts have also been tested in CO_2-FTS.[1] The former materials, however, tend to produce mainly methane, an undesired product, because of their inefficiency to catalyze the RWGS reaction.[5] Fe-based catalysts can produce both CO and C_{2+}-hydrocarbons but also suffer from CH_4 formation.[6] Therefore, it is important to understand fundamentals required for the purposeful development of catalysts with suppressed CH_4 selectivity at industrially relevant degrees of CO_2 conversion.[7] According to our previous statistical analysis of literature data,[8] product selectivity in CO_2-FTS over Fe-based catalysts depends on the kind of promoter for Fe_2O_3, the kind of support, the kind of preparation method of iron oxides and reaction conditions. The fundamentals behind these effects were, however, not clarified.

Alkali metals, acting as electronic and/or structural promoters for improving product selectivity and/or activity, are widely used for preparation of catalysts for various hydrogenation processes, including CO-FTS,[9] ammonia synthesis,[10] selective hydrogenation of alkynes and alkenes,[11] as well as CO_2 hydrogenation.[12] Thus, understanding of origin(s) of their promotional effect is of universal relevance and great interest in the field of heterogeneous catalysis. Sodium or potassium promoters are often reported to reduce CH_4 production in CO_x-FTS over Fe-based catalysts.[13] These promoters are assumed i) to

enhance catalyst basicity required for CO/CO_2 adsorption, ii) to promote the formation of iron carbides and/or iii) to suppress H_2 activation. Such statements were, however, mainly made in studies dealing with one of the above-mentioned aspects. To the best of our knowledge, no systematic studies on the origins of such effects were carried out. There are also controversial conclusions about the effect (positive or negative) of alkali metal promoters on catalyst activity in CO- and CO_2-FTS.[9a,14] Moreover, some fundamental questions remain still unclear, because a major part of previous studies dealt with sodium or potassium promoters.[1a,d] For example, to what extent do the kind and the content of alkali metal promoter influence the formation of iron carbides? Does the presence of iron carbides with or without an alkali metal promoter guarantee low selectivity to CH_4 in favor of desired C_{2+}-hydrocarbons?

Such gap in the fundamental knowledge of CO_2-FTS exists since mechanistic and kinetic aspects of product formation have not been thoroughly elucidated. Rigorous kinetic analysis helps to establish activity–selectivity–property relationships.[15] In particular, spatially resolved kinetic scrutiny allows to understand how reaction rates change along catalyst bed and thus how efficiently catalysts work.[16] Transient techniques have the potential for providing kinetic information on a near to elementary level.[17] Among them, temporal analysis of products (TAP) reactor is a unique technique for such purposes due to analyzing heterogeneous reaction steps with sub-millisecond resolution under isothermal conditions.[18] Although TAP studies are carried out in vacuum, they provide useful information about mechanistic and kinetic aspects of adsorption/desorption/dissociation of feed components and reaction products that are relevant for catalyst activity and product selectivity in various reactions including CO-FTS.[19]

Herein, we elucidate the role of iron carbides in CO_2-FTS and fundamentals affecting their formation/activity to provide basics for purposeful catalyst design. To minimize the contribution of support to the studied reaction, we prepared a series of bulk Fe_2O_3-based catalysts without or with an alkali metal (Li, Na, K, Rb or Cs) promoter. XRD, Mössbauer spectroscopy and X-ray absorption spectroscopy (XAS) were used to analyze the influence of promoter on reaction-induced catalyst restructuring and the relevance of such changes for activity and product selectivity. The fundamentals behind the established differences were rigorously scrutinized through microkinetic analysis of CO_2, CO, C_2H_4 and H_2 activation as well as segmental rate analysis of CO_2 consumption and formation of CH_4 and C_{2+}-hydrocarbons in CO_2-FTS. We show that the reactivity of iron carbides/Fe_3O_4 towards generation of surface species from CO, CO_2 and H_2 correlates with the Allen scale electronegativity of alkali metals, thus, proving their role as electronic promoters. This knowledge may be used for design of catalysts with multiple promoters used not only for CO_2-FTS but also for other hydrogenation reactions.

Results and Discussion

Platform of Catalysts and Reaction-Induced Restructuring

To identify potential descriptors governing catalyst activity and product selectivity in CO_2-FTS, we prepared a series of bulk Fe-based catalysts without or with an alkali metal promoter. They are abbreviated as xAM/Fe (AM: Li, Na, K, Rb or Cs), with x standing for the atomic ratio of the promoter to iron of 0.001, 0.005, 0.02 or 0.05 (Table S1). As-synthesized catalysts are stabilized in the hematite phase (α-Fe_2O_3) as detected by XRD (Figure S1) and TEM (Figure S2). No obvious segregation of promoter species was observed on the surface of α-Fe_2O_3 (Figure S2). Doping of Fe_2O_3 even by small alkali metal amounts (M/Fe = 0.001) slows down the rates of all reduction steps from Fe^{III} to Fe^0 as evidenced by a shift in the maxima of H_2 consumption to higher temperatures in temperature-programmed tests (Figure S3a, b). The shift becomes stronger with an increase in metal loading (Figure S3a, c).

To check if the different performance of 0.001AM/Fe catalysts in CO_2-FTS at a certain contact time (Figure 1a) can be explained by their steady-state composition, we characterized spent samples (after 90 h on reaction stream at 300 °C). Their XRD patterns contain the reflexes characteristic for crystalline Fe_3O_4 and Fe_5C_2 (Figure S4). These phases were also detected by Mössbauer spectroscopy (Figure 1b, c; Figure S5, S6) as well as TEM and SAED analyses (Figure S7). No metallic Fe could be identified by all techniques. This component is present in reduced catalysts but converted into Fe_3O_4 and iron carbides under CO_2-FTS

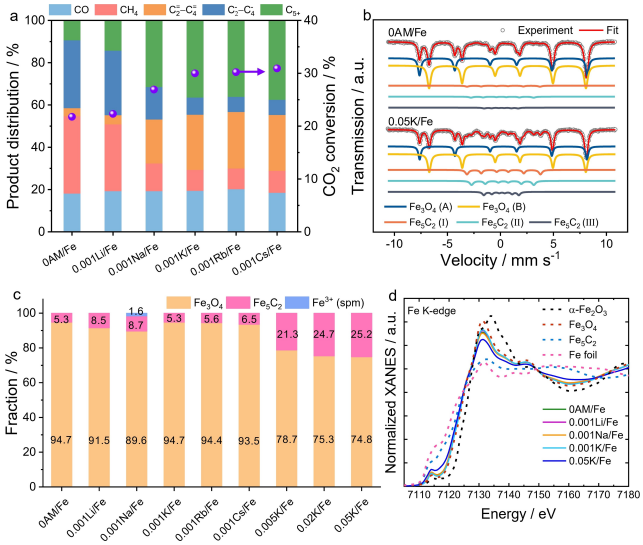

Figure 1. a) CO_2 conversion and product distribution over 0AM/Fe and 0.001AM/Fe catalysts tested in CO_2-FTS at 15 bar and 300 °C using a feed 3 $H_2/CO_2/0.3$ N_2 with a GHSV of 1160 mL g_{cat}^{-1} h^{-1} for 90 h. The catalysts were initially reduced at the same pressure and 400 °C in a mixture of $H_2/N_2 = 1$ for 2 h. b) Mössbauer spectra of spent 0AM/Fe and 0.05 K/Fe catalysts. c) Composition of iron phases in spent catalysts as determined from Mössbauer spectra. d) XANES spectra at Fe K-edge of spent 0AM/Fe, 0.001AM/Fe and 0.05 K/Fe catalysts.

conditions. As both crystalline and X-ray amorphous phases can be analyzed by Mössbauer spectroscopy, we used this technique to quantify the fraction of Fe_5C_2 in spent materials. This fraction in the 0AM/Fe and 0.001AM/Fe catalysts is between 5.3 and 8.7 % (Figure 1c). No direct correlation with the kind of promoter could be established. As exemplarily proven for the K/Fe system, the content of Fe_5C_2 increases from 5.3 to 21.3, 24.7 and 25.2 % with an increase in the K/Fe ratio from 0.001 to 0.005, 0.02 and 0.05, respectively. Thus, promoter concentration is the key factor affecting reaction-induced transformation of Fe_2O_3 to Fe_5C_2.

Figure 1d shows the X-ray absorption near edge structure spectra (XANES) of spent catalysts at the Fe K-edge. They contain a pre-edge feature at 7114 eV that corresponds to the 1s→3d electronic transition.[20] The position of this pre-edge peak and the overall shape of the spectra of 0.001AM/Fe coincide with the Fe_3O_4 reference spectrum. Thus, Fe_3O_4 prevails in the tested samples, that is in line with Mössbauer spectroscopic results (Figure 1c). The spectrum of 0.05 K/Fe shows a higher pre-edge (still at 7114 eV corresponding to both Fe_3O_4 and Fe_5C_2) and lower white line intensities indicating a significant fraction of Fe_5C_2 in a mixture with Fe_3O_4. Extended X-ray absorption fine structure (EXAFS) spectra of spent catalysts are similar to that of Fe_3O_4 (Figure S8). This result further proves the predominantly oxidic nature of iron in 0AM/Fe and 0.001AM/Fe samples. For 0.05 K/Fe catalyst, Fe–O contribution decreases in height and a shoulder at 1.84 Å appears, possibly due to Fe–Fe scattering indicating higher fraction of reduced iron, tentatively in a form of Fe carbide(s).

In summary, although the unpromoted and 0.001AM/Fe spent catalysts possess a similar concentration of Fe_5C_2, they differ strongly in the selectivity to CH_4 and C_{2+}-hydrocarbons at a close degree of CO_2 conversion (Figure 1a). What are the origins behind the effect of alkali metal promoter on product selectivity? To answer this question, we carried out a series of kinetic and mechanistic tests described below.

Effects of Alkali Metal Promoters on Activation of CO_2, CO, C_2H_4 and H_2

Our working hypothesis is that promoters govern the ability of Fe_5C_2 to adsorb/desorb/dissociate CO_2, CO, C_2H_4 and H_2, with these steps being relevant for catalyst activity and product selectivity in CO_2-FTS. The olefin was selected as a probe molecule for investigating adsorption/desorption properties affecting the olefin/paraffin ratio. Pulse experiments were conducted in the TAP reactor at 300 °C with reduced (Fe_3O_4 and metallic Fe coexist) or spent (Fe_3O_4 and Fe_5C_2 coexist, no metallic Fe is present) 0.001AM/Fe catalysts using mixtures of Ar and one of the above-mentioned components with the component ratio of 1. The catalysts with the lowest promoter loading were selected to minimize the contribution of the direct interaction of the promoter with the reactants.

No CO was observed in CO_2/Ar pulse experiments. To check if CO_2 interacts reversibly or irreversibly, we transformed the experimental responses of CO_2 and Ar into a dimensionless form as suggested in Ref. [21]. The dimensionless Ar response stands for pure diffusion process. The CO_2 response crosses the Ar response (Figure S9, S10) irrespective of the absence or the presence of alkali metal promoter as well as of the catalyst state (reduced or spent). This is a fingerprint of reversible adsorption of CO_2. On this basis we developed various microkinetic models (Table S2) and applied them for fitting the experimental CO_2 responses.

The model considering a reversible and dissociative CO_2 adsorption (Scheme 1a) describes the experimental CO_2 responses over reduced and spent catalysts with the smallest deviation (Figure S11–S13; Table S3). The reliability of the obtained kinetic parameters was proven by sensitivity and correlation analyses (Table S4, S5). The reduced and spent catalysts strongly differ in the obtained kinetic parameters of each step (Table S4). Which catalyst components, i.e., Fe (present in reduced catalysts only), Fe_3O_4 (present both in reduced and spent catalysts) or Fe_5C_2 (present in spent catalysts only), mainly contribute to CO_2 activation? Although both reduced and spent catalysts possess mainly Fe_3O_4, they significantly differ in CO_2 desorption profiles and the number of adsorption sites determined from temperature-programmed tests (Figure S14, S15). Thus, Fe_3O_4 does not seem to be the main catalyst component participating in CO_2 activation. The alkali metal promoters are also not exclusively involved in this process, otherwise no differences in the amount of CO_2 desorbed from reduced and spent catalysts could be observed. On this basis, it is proposed that the contribution of Fe_5C_2 (present in spent catalysts) in CO_2 adsorption/activation is higher than that of Fe_3O_4 (present both in reduced and spent catalysts).

As seen in Figure 2, the kind of alkali metal promoter seems to affect the ability of Fe and Fe_5C_2 to adsorb/desorb CO_2 and most importantly to dissociate adsorbed CO_2 species to surface CO and O. Both the $k_{ads}^{eff}(CO_2)$ (an effective adsorption rate constant) and $k_{diss}^{eff}(CO_2)$ (an effective rate constant of dissociation of adsorbed CO_2) values increase in the order 0.001Li/Fe < 0.001Na/Fe < 0.001 K/Fe (Figure 2a, b). In the case of reduced catalysts,

a. Dissociative CO_2 adsorption

$$CO_2 + * \underset{k_{ads}}{\overset{k_{des}}{\rightleftharpoons}} * - CO_2$$

$$* - CO_2 + * \underset{k_{diss}}{\overset{k_{ass}}{\rightleftharpoons}} * - CO + * - O$$

b. Dissociative CO adsorption

$$CO + * \underset{k_{ads}}{\overset{k_{des}}{\rightleftharpoons}} * - CO$$

$$* - CO + * \underset{k_{diss}}{\overset{k_{ass}}{\rightleftharpoons}} * - C + * - O$$

Scheme 1. Microkinetic models of reversible and dissociative adsorption of a) CO_2 and b) CO.

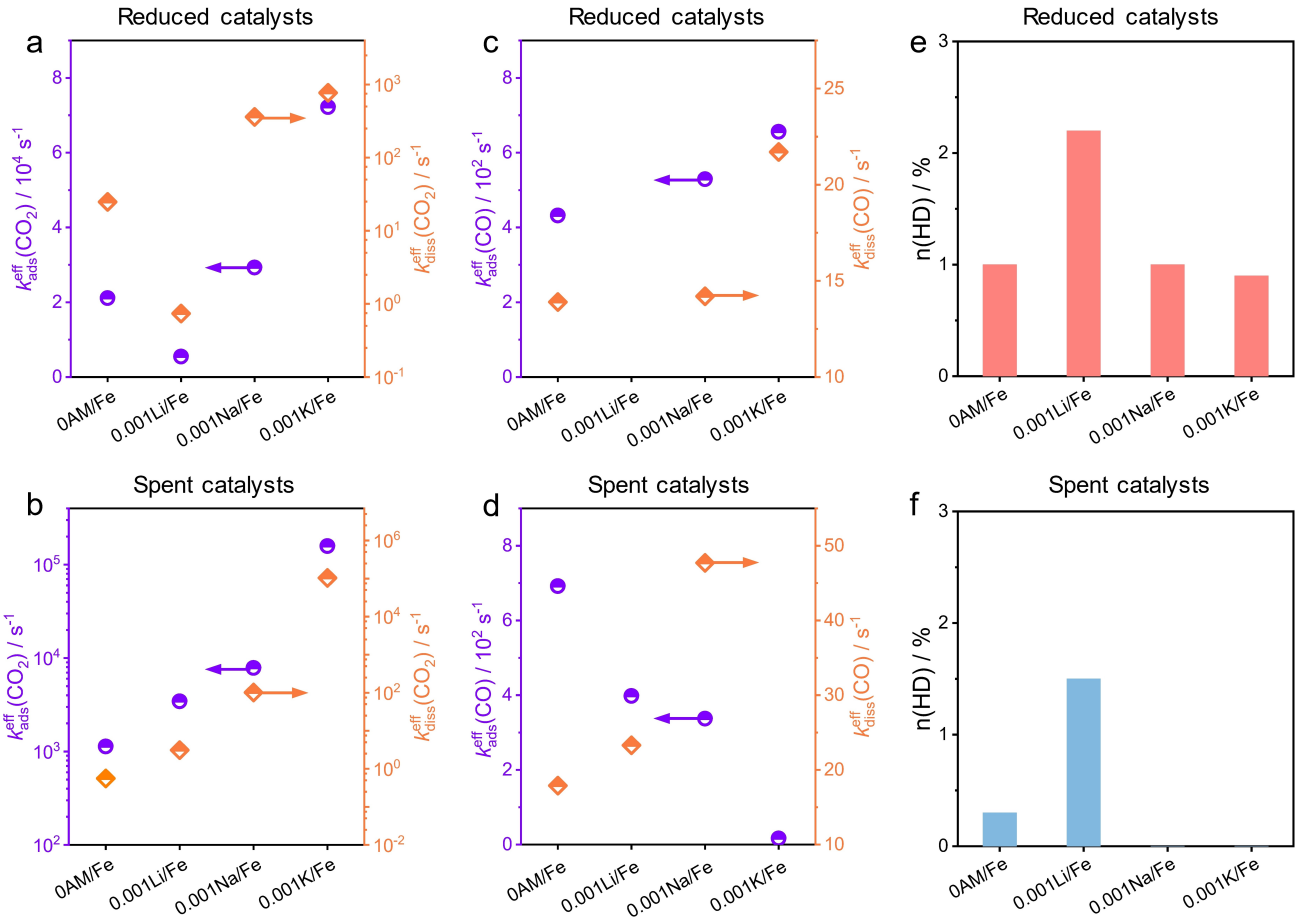

Figure 2. Rate constants of a), b) CO_2 adsorption ($k_{ads}^{eff}(CO_2)$) and dissociation of adsorbed CO_2 ($k_{diss}^{eff}(CO_2)$) (see Scheme 1a), c), d) CO adsorption ($k_{ads}^{eff}(CO)$) and dissociation of adsorbed CO ($k_{diss}^{eff}(CO)$) (Scheme 1b) as well as e), f) fraction of HD determined in H/D exchange experiments at 300 °C. Panels (a), (c), (e) and (b), (d), (f) distinguish reduced and spent catalysts, respectively.

these parameters for 0AM/Fe are higher than those for 0.001Li/Fe (Figure 2a). 0AM/Fe has the lowest values among the spent catalysts (Figure 2b).

Reduced 0.001Li/Fe interacts very weakly with CO because no obvious difference between the dimensionless CO and Ar response could be identified (Figure S16b). Contrarily, CO interacts stronger and reversibly with spent 0.001Li/Fe and with reduced or spent 0AM/Fe, 0.001Na/Fe and 0.001 K/Fe (Figure S16, S17). Simple diffusion model describes satisfactorily the experimental CO response of reduced 0.001Li/Fe but fails for all other reduced or spent catalysts. The model considering a reversible and dissociative CO adsorption (Scheme 1b, Table S6) provides the best fit of the CO responses obtained over these materials (Figure S18, S19; Table S7). The rate constant of CO adsorption ($k_{ads}^{eff}(CO)$) of the reduced 0AM/Fe, 0.001Na/Fe and 0.001 K/Fe materials increases in this order (Figure 2c, Table S8). However, an opposite effect of alkali metal promoter on the rate constant of CO adsorption on the corresponding spent catalysts was established (Figure 2d). If Fe_3O_4, the main component in the reduced and spent materials, contributed to CO adsorption, there would be no difference in the $k_{ads}^{eff}(CO)$ values between these two kinds of catalysts. Thus, metallic Fe and Fe_5C_2 are responsible for CO adsorption but differ in their reactivity. Their ability towards dissociation of adsorbed CO species increases in the presence of alkali metal promoter (Figure 2c, d).

The kind of alkali metal promoter is also relevant for ethylene adsorption. Based on the analysis of dimensionless responses of Ar and C_2H_4 in Figure S20, the promoter (Li, Na or K) affects the strength of ethylene adsorption, which decreases in the order Li > Na > K. The weaker the adsorption, the higher the olefin to paraffin ratio among C_2–C_4 hydrocarbons is (Figure S21).

HD was observed after pulsing of a $H_2/D_2/Ar = 1/1/1$ mixture over reduced or spent catalysts at 300 °C (Figures S22, S23). Its concentration represents the catalyst activity to break the H–H and D–D bonds and to form a new H–D bond. For the reduced catalysts, promoting of Fe_2O_3 with Li enhances H_2 activation, while 0.001Na/Fe and 0.001 K/Fe do not differ from 0AM/Fe in this regard (Figure 2e). Spent 0AM/Fe and 0.001Li/Fe also catalyze the H/D exchange but with a lower activity than their reduced counterparts (Figure 2f). This result suggests that Fe_5C_2 is less active for hydrogen activation than metallic Fe. In comparison with Li,

promoting of Fe_2O_3 with Na or K strongly suppresses the ability of the carbide to activate H_2.

Spatially Resolved Kinetic Analysis of CO_2-FTS

We also investigated how the kind of promoter and its concentration affect the progress of CO_2-FTS along catalyst bed by analyzing segmental rates of overall CO_2 consumption ($r(CO_2)$) and CO_2 conversion into CH_4 ($r(CH_4)$) and C_{2+}-hydrocarbons ($r(C_{2+})$). Figure 3a shows how the segments are defined, while the corresponding formula is given in Equation (1).

$$r_a(CO_2) = \frac{\dot{n}^{a-1}_{CO2} - \dot{n}^{a}_{CO2}}{m^a - m^{a-1}} \text{ or } r_a(i) = \frac{\dot{n}^{a}_{i} - \dot{n}^{a-1}_{i}}{m^a - m^{a-1}} \quad (1)$$

where $\dot{n}$ and m stand for the molar outlet flows of CO_2, CH_4 or C_{2+}-hydrocarbons and catalyst amount, respectively. The superscripts $a-1$ or a are used to distinguish different segments.

$r(CO_2)$ over all catalysts declines downstream from segment to segment due to a decrease in CO_2 partial pressure and accordingly transition from differential to integral reactor (Figure 3b, S24a). The strength of this decrease is highly pronounced for 0AM/Fe, Li/Fe, and Na/Fe but is less noticeable for Rb/Fe, K/Fe and Cs/Fe. Thus, the usage of K, Rb or Cs promoters is advantageous for catalyst efficiency in terms of CO_2 consumption. However, these promoters lower the intrinsic catalyst activity determined in the first catalyst segment ($r_1(CO_2)$), i.e., under differential reactor operation. The following activity order is established: 0AM/Fe ≈ Li/Fe > Na/Fe > Rb/Fe ≈ K/Fe ≈ 1Cs/Fe.

For all catalysts, CH_4 formation mainly occurs within the first 16.7 % upstream-located catalyst layer (Figure 3c, S24b). In terms of CO_2 conversion rate into methane in the first segment ($r_1(CH_4)$), the catalysts can be ordered as follows: 0AM/Fe > Li/Fe ≫ Na/Fe > K/Fe ≈ Rb/Fe ≈ Cs/Fe. This rate over 0AM/Fe and Li/Fe decreases strongly from segment to segment due to an integral reactor operation. The decrease for the catalysts with Na, K, Rb or Cs is less pronounced.

We also determined $r(C_{2+})$ (Figure 3d, S24c). Similar to $r(CO_2)$ and $r(CH_4)$, the highest $r(C_{2+})$ values for 0AM/Fe, Li/Fe and Na/Fe are achieved in the first (about 1.7 %) upstream-located layer. This high activity decreases downstream the catalysts bed strongly due to an integral reactor operation and inhibiting effect of water. This product is known to oxidize iron carbides[7e,22] and to inhibit both RWGS reaction[23] and CO-FTS activity.[24]

$r(C_{2+})$ over K/Fe, Rb/Fe or Cs/Fe passes a maximum between the first 3.3 and 6.7 % of catalyst layers. To compare all the catalysts in terms of their intrinsic activity for CO_2 conversion into C_{2+}-hydrocarbons, we use the $r_1(C_{2+})$ values determined in the first catalyst layer, where

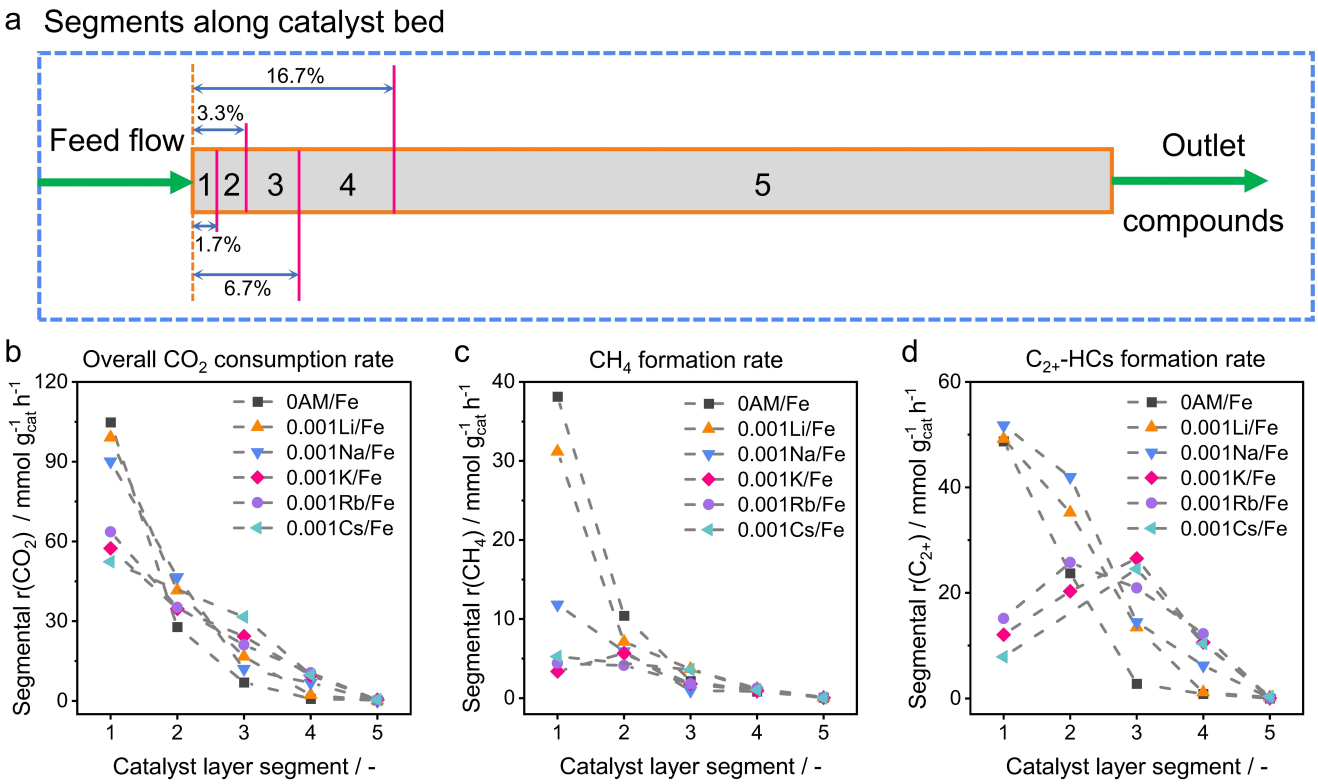

Figure 3. a) Schematic representation how the segments (also see Scheme S1) are defined. The segmental rates of b) overall CO_2 consumption ($r(CO_2)$), c) CH_4 formation ($r(CH_4)$) and d) C_{2+}-hydrocarbons formation ($r(C_{2+})$) over 0AM/Fe and 0.001AM/Fe catalysts. Reaction conditions: $H_2/CO_2/N_2 = 3/1/0.3$, 15 bar and 300 °C.

differential reactor operation can be assumed. The following activity order is obtained: 0AM/Fe≈Li/Fe≈Na/Fe≫K/Fe≈Rb/Fe≈Cs/Fe. As iron carbides catalyze the formation of C_{2+}-hydrocarbons,[7] we can conclude that alkali metal promoters hinder the intrinsic activity of these active species but to a different extent.

Reaction Scheme of Product Formation in CO_2-FTS

Overall scheme of formation of CO, CH_4 and C_{2+}-hydrocarbons in CO_2-FTS was established by analyzing selectivity-conversion relationships for the corresponding products. The relationships were obtained from steady-state tests carried out at different CO_2 conversion degrees. The conversion was varied through changing catalyst amount at a constant total feed flow rate.

CO selectivity has a non-zero value at zero CO_2 conversion and decreases with an increase in the conversion over all catalysts (Figure 4a). This means that CO is directly formed from CO_2 and then consumed in other reactions. To check if CO is hydrogenated to CH_4 we analyze the selectivity-conversion relationship for this product (Figure 4b). This selectivity over 0AM/Fe, 0.001 or 0.05Li/Fe and 0.001 or 0.05Na/Fe does not increase with CO_2 conversion and has a positive value at zero conversion. Thus, CH_4 is not formed over these catalysts from CO but originates mainly through CO_2 hydrogenation. This undesired pathway becomes less important after promoting of α-Fe_2O_3 with Li or Na and is practically totally suppressed

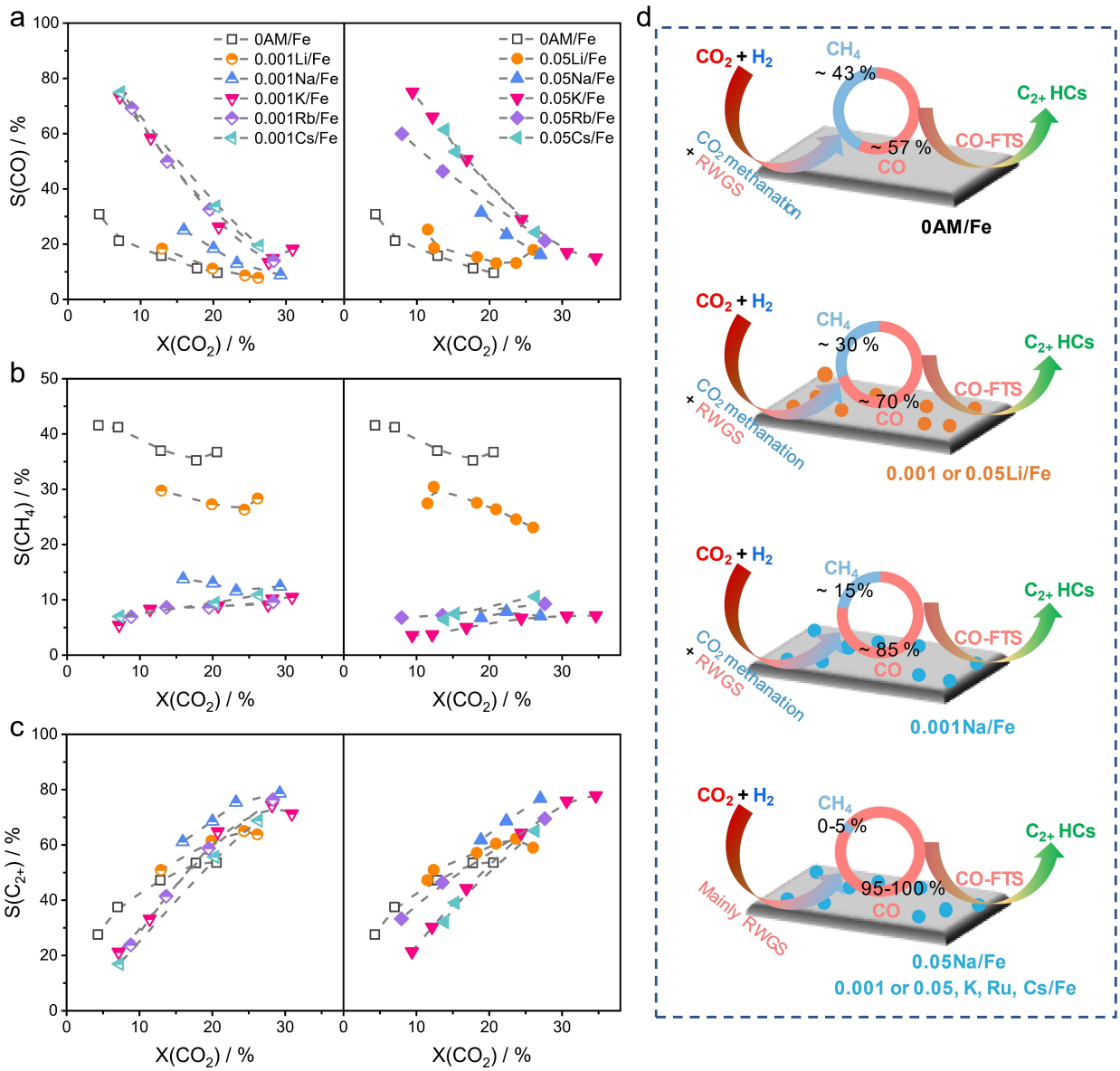

Figure 4. Selectivity–conversion relationships for a) CO, b) CH_4 and c) C_{2+}-hydrocarbons over 0AM/Fe and xAM/Fe catalysts. d) Graphical representation of the reaction scheme of CO_2 conversion. The rings represent the product selectivity at zero CO_2 conversion. Reaction conditions: 300 °C, 15 bar, $H_2/CO_2/N_2 = 3/1/0.3$, after 40 h on stream.

over the catalysts promoted with K, Rb or Cs. Moreover, the higher their loading, the stronger the inhibition is (Figure 4b). CH_4 formation over K/Fe, Rb/Fe and Cs/Fe preferentially occurs with CO participation because the selectivity to CH_4 increases, while the selectivity to CO decreases with an increase in CO_2 conversion. The contribution of direct CO_2 hydrogenation to CH_4 was estimated from the ratio of CH_4 selectivity to CO selectivity at zero CO_2 conversion (Table S10). This ratio is 0.75 for 0AM/Fe and decreases to 0.43, 0.39, 0.18 and 0.05 for 0.001Li/Fe, 0.05Li/Fe, 0.001Na/Fe and 0.05Na/Fe, respectively. Regardless of the concentration of K, Rb or Cs, this ratio is not higher than 0.05.

For all catalysts, CO is also hydrogenated to C_{2+}-hydrocarbons as concluded from the positive effect of CO_2 conversion on the selectivity to these products (Figure 4c). The unpromoted and Li-containing catalysts show higher C_{2+}-selectivity below 20 % CO_2 conversion than the catalysts promoted with other alkali metals (Figure 4c). The selectivity order becomes, however, opposite at higher conversion degrees. The selectivity-conversion profiles for the 0.05AM/Fe catalysts do not principally differ from those of the 0.001AM/Fe catalysts.

When CO_2 conversion increases, the selectivity to light olefins ($C_2^=$–$C_4^=$) passes a maximum but at different CO_2 conversion degrees depending on the kind of promoter (Figure S25). The initial increase indicates that CO is primarily hydrogenated to olefins. They are further hydrogenated to the corresponding alkanes as evidenced by a decrease in the selectivity to the olefins above a certain CO_2 conversion degree. This hydrogenation pathway is hindered by alkali metal promoters. The promoters are ordered according to their inhibition strength as follows $Li \leq Na < K \approx Rb \approx Cs$. With exception for 0.05Li/Fe, no extremum in the selectivity to light olefins could be identified for other catalysts with the AM/Fe of 0.05 (Figure S25b), even in the case of CO_2 conversion beyond 30 % (Figure S26).

In summary, the overall scheme of product formation in CO_2-FTS does not depend on the kind of alkali metal promoter and its loading. The RWGS reaction and CO_2 methanation are two primary reactions running in parallel (Figure 4d). CO is further hydrogenated to CH_4 and C_{2+}-hydrocarbons. The rates of all these pathways are affected by the promoter and its loading. The below analysis is aimed to provide the fundamentals of these effects.

Factors Affecting Activity and Product Selectivity

To rationalize the promoter-dependent changes in catalyst activity (Figure 3, S24) and product selectivity (Figure 4), we combine the spatially resolved and transient kinetics. No correlation could be established between the fraction of iron carbides in 0.001AM/Fe catalysts and product selectivity (Figure 1), while the promoters affect the kinetics of CO, CO_2 and H_2 activation (Figure 2). On this basis, we put forward that electronic interactions between the promoter and Fe_5C_2 are relevant for CO_2-FTS. This assumption is based on several studies stressing the importance of local electronic modifications of Fe through K promoter in NH_3 synthesis[25] or in CO-FTS.[26] Our X-ray photoelectron spectroscopic analysis of spent catalysts supports our hypothesis. The binding energy of Fe in Fe_5C_2 is affected by the kind of alkali metal promoter and its loading (Figure S27). Thus, we suggest using the Allen scale electronegativity of alkali metals as a descriptor representing the electronic promoter effects on activity and product selectivity in CO_2-FTS.

To support this suggestion, we correlated the rates of CO_2 conversion into CH_4 and C_{2+}-hydrocarbons in the first catalyst layer segment (differential reactor operation) with the difference (ΔEN) between the electronegativity of Fe and alkali metal for 0.001AM/Fe (Figure 5a, b) and 0.05AM/Fe (Figure S28a, b) catalysts. These rates decrease with an increase in ΔEN. This correlation can be explained by electronic promoter effects on individual steps of activation of CO_2 and CO. The rate constants of CO_2 adsorption ($k_{ads}^{eff}(CO_2)$, Figure 5c) and dissociation of adsorbed CO_2 ($k_{diss}^{eff}(CO_2)$, Figure S29a) increase with an increase in ΔEN but to a different extent as evidenced by an increase in the ratio of $k_{diss}^{eff}(CO_2)$ to $k_{ads}^{eff}(CO_2)$ (Figure S29b). The equilibrium constant of CO_2 adsorption, that is expressed as $k_{ads}^{eff}(CO_2)/k_{des}(CO_2)$, increases, too.

A negative effect of ΔEN was established for the rate constant of CO adsorption ($k_{ads}^{eff}(CO)$, Figure 5d). Although it was impossible to precisely determine the rate constant of dissociation of adsorbed CO ($k_{diss}^{eff}(CO)$) for 0.001 K/Fe, an

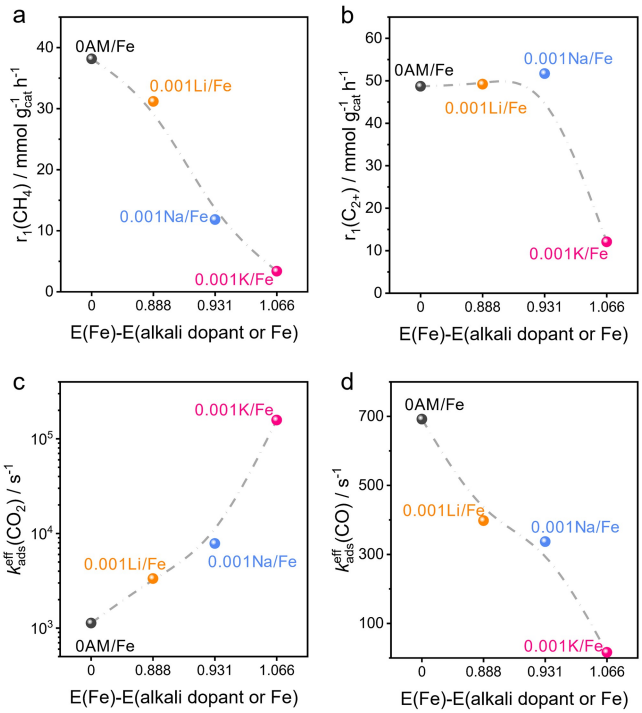

Figure 5. The rates of a) CH_4 ($r_1(CH_4)$) and b) C_{2+}-hydrocarbons ($r_1(C_{2+})$) formation in the first segment (Figure 3a) or the rate constants of adsorption of c) CO_2 ($k_{ads}^{eff}(CO_2)$) and d) CO ($k_{ads}^{eff}(CO)$) determined for spent catalysts at 300 °C versus the difference in the Allen scale electronegativity of iron and alkali metals.

increase in this constant from 0AM/Fe to 0.001Li/Fe and 0.001Na/Fe was established (Figure S30a). Thus, electronic effects seem to be important for breaking the CO bond as indirectly supported by the ratio of $k^{eff}_{diss}(CO)$ to $k^{eff}_{ads}(CO)$ (Figure S30b). They are also essential for the activation of H_2; the H/D exchange catalyst activity decreases with a decrease in the alkali metal electronegativity (Figure S31).

The catalyst ability to activate CO_2 and CO can be correlated with the activity in CO_2-FTS. The rate of CH_4 formation depends on the ratio of $k^{eff}_{diss}(CO_2)/k^{eff}_{ads}(CO_2)$, which determines the ability of catalysts to generate surface species from CO_2 (Figure S32a). In the case of C_{2+}-hydrocarbons, their formation rate increases with $k^{eff}_{ads}(CO)$ (Figure S32b). Moreover, the overall rate of CO_2 consumption decreases with an increase in the $k^{eff}_{ads}(CO_2)/k_{des}(CO_2)$ ratio (Figure S33). Too strong CO_2 adsorption seems to be detrimental for catalyst activity.

From a selectivity viewpoint, the promoters affect local electronic sate of iron in iron carbides (Figure S34) that is important for CO_2 activation. Dissociation of adsorbed CO species into the individual surface components is also influenced. The stronger the electronic effect of the promoter, the higher the adsorption strength of CO_2 is. This results in an increase in the coverage by C-containing species. Contrarily, the catalyst ability to generate surface hydrogen species from gas-phase H_2 and to adsorb CO is inhibited. Olefin adsorption is also hindered. Such multi-effects have consequences for product selectivity because the surface C/H ratio depends on the kinetics of the above interactions. A suitable ratio is required for inhibiting CH_4 formation, for the selective production of C_{2+}-hydrocarbons and for hindering consecutive hydrogenation of primarily formed olefins to paraffins.

Conclusion

Unlike traditionally applied one-contact time measurements for determining reaction rates or overall catalyst activity in CO_2-FTS, spatially resolved kinetic analysis enabled us to compare Fe-based catalysts in terms of their intrinsic activity and to determine how the rates change along catalyst bed. In comparison with iron carbides present in the unpromoted catalyst, Li or Na promoters does not practically affect the activity of iron carbides to produce C_{2+}-hydrocarbons, while K, Rb or Cs promoters worsen this catalyst property significantly. The rate of CH_4 formation is hindered even stronger. Although the overall concentration of iron carbides does not depend on the kind of promoter, the K, Rb or Cs promoters are important for spatial distribution of these active species along the catalyst bed and thus for improving catalyst efficiency to produce C_{2+}-hydrocarbons.

The effects of alkali metal promoters were explained by local electronic modifications of iron in iron carbides. The Allen scale electronegativity of the promoters can be used as a descriptor determining both activity and product selectivity. The effectiveness of this descriptor was also proved by the kinetic analysis of CO, CO_2 and H_2 activation. It suggests that promoters with lower energy of the valence electrons hinder catalyst ability to adsorb CO and H_2 but increase CO_2 adsorption and dissociation. Thus, we provide fundamentals for tailored design of Fe-based catalysts that can also be applicable beyond this reaction.

Acknowledgements

This work was funded by the Deutsche Forschungsgemeinschaft (DFG) under the priority program SPP 2080 (grants no. KO 2261/10-1, KO 2261/10-2). Financial support from the Leibniz-Gemeinschaft e. V. is also acknowledged (SAW-2017-LIKAT-1). The authors thank Dr. Stephan Bartling for X-ray photoelectron spectroscopic analyses. The authors acknowledge DESY (Hamburg, Germany), a member of the Helmholtz Association HGF, for providing the experimental facilities. Parts of this research were carried out at PETRA III and we would like to thank Dr. Morgane Desmau and Dr. Edmund Welter for their assistance in using beamline P65. The authors gratefully acknowledge the efforts of Frau Laura Kraußer for translating the English original manuscript into German. Open Access funding enabled and organized by Projekt DEAL.

Conflict of Interest

The authors declare no conflict of interest.

Data Availability Statement

The data that support the findings of this study are available from the corresponding author upon reasonable request.

Keywords: CO_2 Utilization · Heterogeneous Catalysis · Hydrogenation · Iron · Kinetics

[1] a) W. Wang, S. P. Wang, X. B. Ma, J. L. Gong, *Chem. Soc. Rev.* **2011**, *40*, 3703–3727; b) E. V. Kondratenko, G. Mul, J. Baltrusaitis, G. O. Larrazábal, J. Pérez-Ramírez, *Energy Environ. Sci.* **2013**, *6*, 3112–3135; c) M. D. Burkart, N. Hazari, C. L. Tway, E. L. Zeitler, *ACS Catal.* **2019**, *9*, 7937–7956; d) R. P. Ye, J. Ding, W. Gong, M. D. Argyle, Q. Zhong, Y. Wang, C. K. Russell, Z. Xu, A. G. Russell, Q. Li, M. Fan, Y. G. Yao, *Nat. Commun.* **2019**, *10*, 5698; e) X. Jiang, X. Nie, X. Guo, C. Song, J. G. Chen, *Chem. Rev.* **2020**, *120*, 7984–8034.

[2] a) A. Ramirez, A. Dutta Chowdhury, A. Dokania, P. Cnudde, M. Caglayan, I. Yarulina, E. Abou-Hamad, L. Gevers, S. Ould-Chikh, K. De Wispelaere, V. van Speybroeck, J. Gascon, *ACS Catal.* **2019**, *9*, 6320–6334; b) J. Zhu, G. Zhang, W. Li, X. Zhang, F. Ding, C. Song, X. Guo, *ACS Catal.* **2020**, *10*, 7424–7433; c) C. Yang, C. Pei, R. Luo, S. Liu, Y. Wang, Z. Wang, Z.-J. Zhao, J. Gong, *J. Am. Chem. Soc.* **2020**, *142*, 19523–19531; d) A. Parastaev, V. Muravev, E. H. Osta, A. J. van Hoof, T. F. Kimpel, N. Kosinov, E. J. Hensen, *Nat. Catal.* **2020**, *3*, 526–533; e) X. Li, J. Lin, L. Li, Y. Huang, X. Pan, S. E. Collins, Y. Ren, Y. Su, L. Kang, X. Liu, *Angew. Chem. Int. Ed.* **2020**, *59*, 19983–19989; *Angew. Chem.* **2020**, *132*, 20158–20164.

[3] a) S. Dang, S. Li, C. Yang, X. Chen, X. Li, L. Zhong, P. Gao, Y. Sun, *ChemSusChem* **2019**, *12*, 3582–3591; b) X. Liu, M. Wang, H. Yin, J. Hu, K. Cheng, J. Kang, Q. Zhang, Y. Wang, *ACS Catal.* **2020**, *10*, 8303–8314.

[4] a) T. Riedel, G. Schaub, K. W. Jun, K. W. Lee, *Ind. Eng. Chem. Res.* **2001**, *40*, 1355–1363; b) Y. H. Choi, Y. J. Jang, H. Park, W. Y. Kim, Y. H. Lee, S. H. Choi, J. S. Lee, *Appl. Catal. B* **2017**, *202*, 605–610; c) J. Liu, A. Zhang, X. Jiang, M. Liu, Y. Sun, C. Song, X. Guo, *ACS Sustainable Chem. Eng.* **2018**, *6*, 10182–10190; d) S. Geng, F. Jiang, Y. Xu, X. Liu, *ChemCatChem* **2016**, *8*, 1303–1307.

[5] a) R. A. Fiato, E. Iglesia, G. W. Rice, S. L. Soled, *Stud. Surf. Sci. Catal.* **1998**, *114*, 339–344; b) Y. Zhang, G. Jacobs, D. E. Sparks, M. E. Dry, B. H. Davis, *Catal. Today* **2002**, *71*, 411–418; c) R. Satthawong, N. Koizumi, C. Song, P. Prasassarakich, *J. CO2 Util.* **2013**, *3–4*, 102–106.

[6] a) A. Ramirez, L. Gevers, A. Bavykina, S. Ould-Chikh, J. Gascon, *ACS Catal.* **2018**, *8*, 9174–9182; b) M. Albrecht, U. Rodemerck, M. Schneider, M. Bröring, D. Baabe, E. V. Kondratenko, *Appl. Catal. B* **2017**, *204*, 119–126.

[7] a) J. Wei, Q. Ge, R. Yao, Z. Wen, C. Fang, L. Guo, H. Xu, J. Sun, *Nat. Commun.* **2017**, *8*, 15174; b) A. Aitbekova, E. D. Goodman, L. Wu, A. Boubnov, A. S. Hoffman, A. Genc, H. Cheng, L. Casalena, S. R. Bare, M. Cargnello, *Angew. Chem. Int. Ed.* **2019**, *58*, 17451–17457; *Angew. Chem.* **2019**, *131*, 17612–17618; c) Y. Han, C. Fang, X. Ji, J. Wei, Q. Ge, J. Sun, *ACS Catal.* **2020**, *10*, 12098–12108; d) B. Yao, T. Xiao, O. A. Makgae, X. Jie, S. Gonzalez-Cortes, S. Guan, A. I. Kirkland, J. R. Dilworth, H. A. Al-Megren, S. M. Alshihri, P. J. Dobson, G. P. Owen, J. M. Thomas, P. P. Edwards, *Nat. Commun.* **2020**, *11*, 6395; e) A. S. Skrypnik, Q. Yang, A. A. Matvienko, V. Y. Bychkov, Y. P. Tulenin, H. Lund, S. A. Petrov, R. Kraehnert, A. Arinchtein, J. Weiss, *Appl. Catal. B* **2021**, *291*, 120121.

[8] Q. Yang, A. Skrypnik, A. Matvienko, H. Lund, M. Holena, E. V. Kondratenko, *Appl. Catal. B* **2021**, *282*, 119554.

[9] a) H. Arakawa, A. T. Bell, *Ind. Eng. Chem. Process Des. Dev.* **1983**, *22*, 97–103; b) W. Ngantsoue-Hoc, Y. Zhang, R. J. O'Brien, M. Luo, B. H. Davis, *Appl. Catal. A* **2002**, *236*, 77–89; c) Z. Li, L. Zhong, F. Yu, Y. An, Y. Dai, Y. Yang, T. Lin, S. Li, H. Wang, P. Gao, Y. Sun, M. He, *ACS Catal.* **2017**, *7*, 3622–3631.

[10] a) G. Ertl, S. B. Lee, M. Weiss, *Surf. Sci.* **1982**, *114*, 527–545; b) J. J. Mortensen, B. Hammer, J. K. Nørskov, *Phys. Rev. Lett.* **1998**, *80*, 4333–4336; c) Q. Wang, J. Guo, P. Chen, *Chem* **2021**, *7*, 3203–3220.

[11] a) A. Borodziński, G. C. Bond, *Catal. Rev.* **2008**, *50*, 379–469; b) S. A. Mavlyankariev, S. J. Ahlers, V. A. Kondratenko, D. Linke, E. V. Kondratenko, *ACS Catal.* **2016**, *6*, 3317–3325.

[12] a) M. Amoyal, R. Vidruk-Nehemya, M. V. Landau, M. Herskowitz, *J. Catal.* **2017**, *348*, 29–39; b) U. Rodemerck, M. Holeňa, E. Wagner, Q. Smejkal, A. Barkschat, M. Baerns, *ChemCatChem* **2013**, *5*, 1948–1955; c) X. Yang, X. Su, X. Chen, H. Duan, B. Liang, Q. Liu, X. Liu, Y. Ren, Y. Huang, T. Zhang, *Appl. Catal. B* **2017**, *216*, 95–105.

[13] a) J. Wang, Z. You, Q. Zhang, W. Deng, Y. Wang, *Catal. Today* **2013**, *215*, 186–193; b) R. Satthawong, N. Koizumi, C. Song, P. Prasassarakich, *Catal. Today* **2015**, *251*, 34–40; c) W. D. Shafer, G. Jacobs, U. M. Graham, H. H. Hamdeh, B. H. Davis, *J. Catal.* **2019**, *369*, 239–248; d) B. Liang, H. Duan, T. Sun, J. Ma, X. Liu, J. Xu, X. Su, Y. Huang, T. Zhang, *ACS Sustainable Chem. Eng.* **2019**, *7*, 925–932; e) J. Wei, J. Sun, Z. Wen, C. Fang, Q. Ge, H. Xu, *Catal. Sci. Technol.* **2016**, *6*, 4786–4793; f) Y. Xu, P. Zhai, Y. Deng, J. Xie, X. Liu, S. Wang, D. Ma, *Angew. Chem. Int. Ed.* **2020**, *59*, 21736–21744; *Angew. Chem.* **2020**, *132*, 21920–21928; g) L. Guo, J. Li, Y. Cui, R. Kosol, Y. Zeng, G. Liu, J. Wu, T. Zhao, G. Yang, L. Shao, P. Zhan, J. Chen, N. Tsubaki, *Chem. Commun.* **2020**, *56*, 9372–9375.

[14] a) A. P. Raje, R. J. O'Brien, B. H. Davis, *J. Catal.* **1998**, *180*, 36–43; b) H. M. Torres Galvis, A. C. J. Koeken, J. H. Bitter, T. Davidian, M. Ruitenbeek, A. I. Dugulan, K. P. de Jong, *J. Catal.* **2013**, *303*, 22–30; c) H. S. Malhi, C. Sun, Z. Zhang, Y. liu, W. Liu, P. Ren, W. Tu, Y.-F. Han, *Catal. Today* **2022**, *387*, 28–37.

[15] a) A. H. Motagamwala, J. A. Dumesic, *Chem. Rev.* **2021**, *121*, 1049–1076; b) E. V. Kondratenko, *Catal. Today* **2010**, *157*, 16–23; c) S. Matera, W. F. Schneider, A. Heyden, A. Savara, *ACS Catal.* **2019**, *9*, 6624–6647.

[16] a) B. Wollak, D. E. Doronkin, D. Espinoza, T. Sheppard, O. Korup, M. Schmidt, S. Alizadefanaloo, F. Rosowski, C. Schroer, J. D. Grunwaldt, R. Horn, *J. Catal.* **2022**, https://doi.org/10.1016/j.jcat.2021.08.029; b) M.-A. Serrer, M. Stehle, M. L. Schulte, H. Besser, W. Pfleging, E. Saraçi, J.-D. Grunwaldt, *ChemCatChem* **2021**, *13*, 3010–3020; c) K. Morgan, J. Touitou, J.-S. Choi, C. Coney, C. Hardacre, J. A. Pihl, C. E. Stere, M.-Y. Kim, C. Stewart, A. Goguet, W. P. Partridge, *ACS Catal.* **2016**, *6*, 1356–1381.

[17] a) E. V. Kondratenko, *Top. Catal.* **2013**, *56*, 858–866; b) C. Ledesma, J. Yang, D. Chen, A. Holmen, *ACS Catal.* **2014**, *4*, 4527–4547.

[18] a) G. Yablonsky, M. Olea, G. Marin, *J. Catal.* **2003**, *216*, 120–134; b) J. Pérez-Ramírez, E. V. Kondratenko, *Catal. Today* **2007**, *121*, 160–169.

[19] a) D. Widmann, R. J. Behm, *Acc. Chem. Res.* **2014**, *47*, 740–749; b) K. Morgan, N. Maguire, R. Fushimi, J. Gleaves, A. Goguet, M. Harold, E. Kondratenko, U. Menon, Y. Schuurman, G. Yablonsky, *Catal. Sci. Technol.* **2017**, *7*, 2416–2439; c) V. A. Kondratenko, C. Berger-Karin, E. V. Kondratenko, *ACS Catal.* **2014**, *4*, 3136–3144; d) M. A. G. Hevia, A. P. Amrute, T. Schmidt, J. Pérez-Ramírez, *J. Catal.* **2010**, *276*, 141–151; e) M. Baerns, R. Imbihl, V. A. Kondratenko, R. Kraehnert, W. K. Offermans, R. A. van Santen, A. Scheibe, *J. Catal.* **2005**, *232*, 226–238; f) Y. Qi, J. Yang, D. Chen, A. Holmen, *Catal. Lett.* **2015**, *145*, 145–161.

[20] A. Boubnov, H. Lichtenberg, S. Mangold, J.-D. Grunwaldt, *J. Synchrotron Radiat.* **2015**, *22*, 410–426.

[21] J. T. Gleaves, G. S. Yablonskii, P. Phanawadee, Y. Schuurman, *Appl. Catal. A* **1997**, *160*, 55–88.

[22] E. de Smit, B. M. Weckhuysen, *Chem. Soc. Rev.* **2008**, *37*, 2758–2781.

[23] S. Saeidi, S. Najari, F. Fazlollahi, M. K. Nikoo, F. Sefidkon, J. J. Klemeš, L. L. Baxter, *Renewable Sustainable Energy Rev.* **2017**, *80*, 1292–1311.

[24] a) C. N. Satterfield, R. T. Hanlon, S. E. Tung, Z. M. Zou, G. C. Papaefthymiou, *Ind. Eng. Chem. Prod. Res. Dev.* **1986**, *25*, 407–414; b) H. Schulz, *Appl. Catal. A* **1999**, *186*, 3–12.

[25] a) R. Schlögl in *Handbook of Heterogeneous Catalysis* (Eds.: G. Ertl, H. Knözinger, F. Schüth, J. Weitkamp), Wiley-VCH, Weinheim, **2008**, pp. 2501–2575; b) G. A. Somorjai, N. Materer, *Top. Catal.* **1994**, *1*, 215–231.

[26] a) G. P. Van Der Laan, A. A. C. M. Beenackers, *Catal. Rev.* **1999**, *41*, 255–318; b) Q. Zhang, J. Kang, Y. Wang, *ChemCatChem* **2010**, *2*, 1030–1058.

Manuscript received: December 3, 2021
Accepted manuscript online: March 4, 2022
Version of record online: March 31, 2022